Topography of acute stroke in a sample of 439 right brain damaged patients

Article *in* NeuroImage: Clinical · November 2015

DOI: 10.1016/j.nicl.2015.11.012

CITATIONS
41

READS
90

2 authors:

Christoph Sperber
Inselspital, Universitätsspital Bern
42 PUBLICATIONS **677** CITATIONS

SEE PROFILE

Hans-Otto Karnath
University of Tuebingen
347 PUBLICATIONS **19,353** CITATIONS

SEE PROFILE

NeuroImage: Clinical 10 (2016) 124–128

Contents lists available at ScienceDirect

NeuroImage: Clinical

journal homepage: www.elsevier.com/locate/ynicl

Topography of acute stroke in a sample of 439 right brain damaged patients

Christoph Sperber [a], Hans-Otto Karnath [a,b,*]

[a] Center of Neurology, Division of Neuropsychology, Hertie-Institute for Clinical Brain Research, University of Tübingen, Tübingen, Germany
[b] Department of Psychology, University of SC, Columbia, USA

ARTICLE INFO

Article history:
Received 5 August 2015
Received in revised form 26 October 2015
Accepted 16 November 2015
Available online 17 November 2015

Keywords:
Lesion mapping
Infarct
Lesion size
Hemorrhage
Volumetry

ABSTRACT

Knowledge of the typical lesion topography and volumetry is important for clinical stroke diagnosis as well as for anatomo-behavioral lesion mapping analyses. Here we used modern lesion analysis techniques to examine the naturally occurring lesion patterns caused by ischemic and by hemorrhagic infarcts in a large, representative acute stroke patient sample. Acute MR and CT imaging of 439 consecutively admitted right-hemispheric stroke patients from a well-defined catchment area suffering from ischemia ($n = 367$) or hemorrhage ($n = 72$) were normalized and mapped in reference to stereotaxic anatomical atlases. For ischemic infarcts, highest frequencies of stroke were observed in the insula, putamen, operculum and superior temporal cortex, as well as the inferior and superior occipito-frontal fascicles, superior longitudinal fascicle, uncinate fascicle, and the acoustic radiation. The maximum overlay of hemorrhages was located more posteriorly and more medially, involving posterior areas of the insula, Heschl's gyrus, and putamen. Lesion size was largest in frontal and anterior areas and lowest in subcortical and posterior areas. The large and unbiased sample of stroke patients used in the present study accumulated the different sub-patterns to identify the global topographic and volumetric pattern of right hemisphere stroke in humans.

1. Introduction

The area of damaged tissue in stroke follows patterns determined by the structure of the vascular trees (Stoeckel et al., 2007; Lee et al., 2009). Knowledge of typical lesion patterns is crucial in clinical stroke diagnosis as well as in anatomo-behavioral studies using statistical techniques such as voxel-based lesion-behavior mapping (Bates et al., 2003; Rorden et al., 2007). Nonetheless, studies describing the anatomy of brain damage are rare and often focused on subpopulations of strokes as for example patients with aphasia (Mirman et al., 2015; Caviness et al., 2002), included small sample sizes, and/or were based on acute perfusion MRI (Stoeckel et al., 2007; Caviness et al., 2002; Phan et al., 2005, 2007), which is not necessarily equivalent to final lesion demarcation (Neumann-Haefelin et al., 1999). A study by Lee et al. investigated a large sample of 205 patients. (Lee et al., 2009) Their results lacked a detailed topography as they concentrated on a binary classification (lesioned vs. non-lesioned) of large regions of interest (ROIs). Moreover, the study was restricted to infarcts of the PCA territory. To our knowledge the largest sample of lesion data has recently been published by Mah et al. (2014). The authors evaluated 581 left or right hemispheric stroke patients who had obtained diffusion weighted MR imaging, covering all vascular trees. Unfortunately, no descriptive information (location, size, phase of stroke, etc.) from the lesion groups and the illustrated anatomical overlay was provided.

The present study aimed to analyze a large, representative sample of stroke patients and describes lesion size and topography caused by ischemic and by hemorrhagic infarcts. To avoid any loss of representativeness individuals should be included independent of the imaging modality applied at admission. The latter is of relevance since in many stroke centers, a dominant brain imaging method applied at admission is CT with advantages typically including speed, cost, and reduced exclusion criteria relative to MRI. In clinical routine, there is a tendency to examine patients with severe and clear stroke symptoms at admission by CT imaging, since the dominant interest in those cases is to quickly identify hemorrhages. Contingent upon individual on-site organization achievement of this purpose is often faster and definitely cheaper by CT than by MR imaging. To exclude a systematic bias of our sample towards patients with less severe and less clear symptoms

* Corresponding author at: Center of Neurology, University of Tübingen, 72076 Tübingen, Germany.
E-mail address: Karnath@uni-tuebingen.de (H.-O. Karnath).

http://dx.doi.org/10.1016/j.nicl.2015.11.012

on admission, the present analysis should be based not only on acute MR but also on acute CT imaging.

2. Methods

2.1. Patient selection

Neurological patients admitted between 1999 and 2013 to the Centre of Neurology at Tübingen University Hospital were screened for an acute first unilateral, right-hemispheric stroke as indicated either by magnetic resonance (MR) imaging or computed tomography (CT). Patients with left-hemisphere stroke, with diffuse, bilateral, or cerebellar brain lesions, with previous large-artery or embolic stroke or pathological morphological changes of brain anatomy (e.g. massive brain atrophy), patients with tumors, patients with marked anatomical distortion due to intracerebral bleeding, patients who did not survive the acute stage of stroke, and patients without obvious lesion shown in MRI or CT were excluded. We included 439 patients (188 f, 251 m) with an average age of 62.4 years (SD = 13.4) at stroke onset. Of these patients, 367 had an infarct and 72 a hemorrhage. All patients or their relatives gave informed consent to participate in our study, which was performed according to the ethical standards laid down in the 1964 Declaration of Helsinki.

2.2. Imaging and lesion mapping

For all patients, an acute lesion was demonstrated by either CT or MR imaging. If both scan modalities were available, MR scans were preferred. As the validity to accurately identify stroke differs between imaging modalities dependent on time since stroke, under both protocols the initial scanning optionally was repeated during the following days until a firm diagnosis could be made and the infarcted area became clearly demarcated such that a clinically experienced researcher or a clinician experienced in lesion mapping could clearly identify lesion borders. The final scans were used for the present study. The present study included lesions that were demonstrated by using MR imaging in 210 cases and by CT in 229 cases. Time between stroke onset and imaging was 4.2 days (SD = 7.0) on average. In the subjects who underwent MRI scanning, we used diffusion-weighted imaging (DWI) in the hyper-acute phase until 48 h after stroke onset and T_2-weighted fluid attenuated inversion recovery (FLAIR) imaging in later stages after stroke onset.

For a majority of patients ($n = 274$) CT or MR imaging data were available in digital format. For these patients, the lesion was manually delineated on axial slices of the individual CT or MR scans using MRIcron (www.mccauslandcenter.sc.edu/mricro/mricron). Normalization of CT or MR scans was performed by using the Clinical Toolbox (Rorden et al., 2012) under SPM8 (www.fil.ion.ucl.ac.uk/spm), which provides age-specific templates oriented in MNI space for both CT and MR scans. If available, the MR scans were co-registered with a high-resolution T_1-weighted structural scan in the normalization process. For the remaining patients ($n = 165$) admitted before digital scans became available, lesions were drawn manually on slices of the T_1-weighted 'ch2' template MRI from the Montreal Neurological Institute (www.bic.mni.mcgill.ca/cgi/icbm_view) which is distributed with MRIcron. For the slices with the z-coordinates −40, −32, −24,

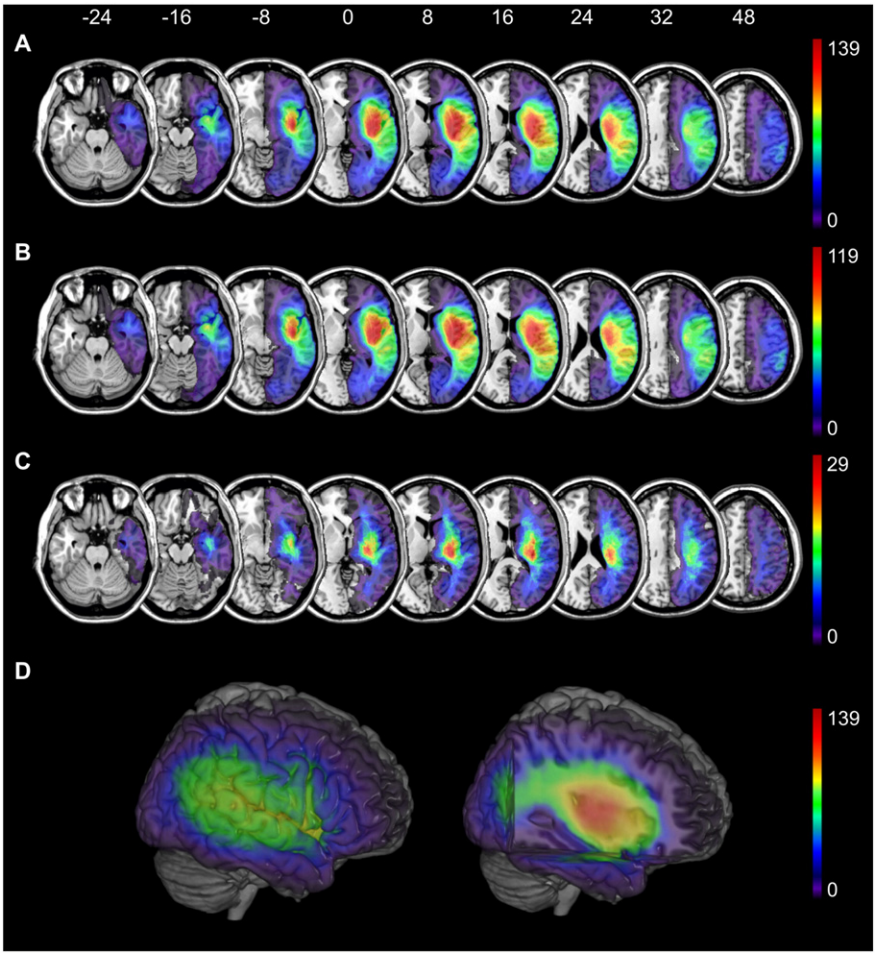

Fig. 1. Simple overlay plots for (A) all 439 acute right brain damaged patients, (B) for infarcts only ($n = 367$), (C) for hemorrhages only ($n = 72$), and (D) a 3D-rendered overlay plot for all 439 acute right brain damaged patients.

−16, −8, 0, 8, 16, 24, 32, 40, and 50 mm in MNI space lesions were drawn using the identical or closest matching transversal slice of each individual. To compute an estimate for lesion size in these cases, the build-in interpolation algorithm of MRIcron was used. Delineation of lesion borders was verified by consensus of two experienced investigators.

Region-based analyses of cortical lesion anatomy were carried out using the Automatic Anatomical Labeling atlas (AAL) distributed with MRIcron (Tzourio-Mazoyer et al., 2002). White matter structures were analyzed with the white matter fiber tract templates from the Jülich probabilistic cytoarchitectonic atlas (Bürgel et al., 2006). Regions of interest were defined as voxels with a relative frequency to belong to a certain fiber tract of ≥30%. All analyses were performed by using the MRIcron software package and the 'Tools for NIFTI and ANALYZE image' Toolkit (http://www.mathworks.com/matlabcentral/fileexchange/8797-tools-for-nifti-and-analyze-image) in MATLAB 2009. All resulting topographies were illustrated on the 'ch2' template set in MNI space.

3. Results

The overlay lesion plot of the 439 patients showed a wide distribution of lesions covering the whole right hemisphere (Fig. 1). Overall normalized lesion size was 52.2 cm^3 (SD = 60.1; median 31.9 cm^3; 25%-quantile 9.4 cm^3; 75%-quantile 72.9 cm^3), while infarcts were 54.1 cm^3 (SD = 63.4) and hemorrhages 42.9 cm^3 (SD = 38.2) in size. Table 1 gives an overview of the percentage of affection of cortical and subcortical gray and white matter structures. The maximum was located in the territory of the middle cerebral artery (MCA). Within this territory, we observed the highest frequencies of affection in the insula, putamen, operculum, and superior temporal cortex, as well as the inferior and superior occipito-frontal fascicles, superior longitudinal fascicle, uncinate fascicle, and the acoustic radiation. This maximum overlay was mainly due to infarcts (Fig. 1b); the maximum overlay of hemorrhages was found in a more posterior and medial region (Fig. 1c), involving posterior areas of the insula, Heschl's gyrus, and putamen.

In order to compute a topography for lesion size, we identified for every voxel that was affected in at least $n = 5$ patients all individual lesions that included this voxel. We then averaged the size of these lesions to compute an estimate for the average size of lesions that affected this voxel. A lesion size topography for all 439 patients (Fig. 2a) showed that lesions affecting occipital areas were smaller than those affecting other regions; lesions reaching into prefrontal cortex tended to be the largest. Again, this distribution was mainly due to infarcts (Fig. 2b). The lesion size topography of hemorrhages (Fig. 2c) showed that hemorrhages affecting the thalamus were smallest; maxima were observed in several cortical and subcortical areas, most notably in the pre- and post-central gyri and the prefrontal cortex.

For a more detailed view within the MCA territory, we changed map scaling to account for the variation within this area only (Fig. 2d). This map showed that inside the MCA territory lesions affecting subcortical structures including the putamen, pallidum and insula, tended to be the smallest. There was a tendency for lesions to increase in size as they were located more cortically. In particular, the pre- and post-central gyri as well as prefrontal and anterior temporal cortices were typically affected by lesions of larger size.

Table 1
Averaged stroke frequency and lesion size for cortical and subcortical regions of interest, including all 439 acute right brain damaged patients. Gray matter areas are in reference to the AAL atlas, white matter areas in reference to the Jülich atlas (probability of p ≥ 30% for the latter). Average overlay is the mean percentage of affection of each area over all lesions. Average lesion size is the mean volume of lesions affecting an area, as obtained for the size lesion plot (Fig. 2a) and averaged over all voxels in the area. (The same table can be found for infarcts and hemorrhages separately in online Supplementary Tables 1 and 2.)

Area	Average overlay in %	Area	Average lesion size in cm^3
Gray matter structures			
Heschl_R	22.35	Frontal_Inf_Orb_R	143.86
Insula_R	21.54	Amygdala_R	130.89
Putamen_R	21.23	Temporal_Pole_Mid_R	130.49
Rolandic_Oper_R	19.12	Temporal_Pole_Sup_R	129.55
Temporal_Sup_R	16.21	Frontal_Mid_R	129.39
Pallidum_R	14.17	SupraMarginal_R	127.26
Frontal_Inf_Oper_R	13.07	Temporal_Sup_R	125.14
SupraMarginal_R	12.62	Rolandic_Oper_R	124.77
Temporal_Mid_R	11.37	Frontal_Inf_Tri_R	124.17
Caudate_R	9.43	Frontal_Inf_Oper_R	123.47
Angular_R	9.23	Heschl_R	122.34
Amygdala_R	8.60	Precentral_R	121.59
Frontal_Inf_Tri_R	7.67	Temporal_Mid_R	120.57
Parietal_Inf_R	7.59	Frontal_Mid_Orb_R	120.08
Temporal_Pole_Sup_R	7.02	Insula_R	119.53
Occipital_Mid_R	6.51	Pallidum_R	113.27
Precentral_R	5.99	Postcentral_R	112.25
Frontal_Inf_Orb_R	5.99	Parietal_Inf_R	111.59
Hippocampus_R	5.96	Temporal_Inf_R	106.77
Postcentral_R	5.54	Angular_R	103.09
Calcarine_R	5.50	Putamen_R	102.46
Lingual_R	4.61	Caudate_R	102.42
Occipital_Inf_R	4.22	Frontal_Sup_R	101.77
Temporal_Inf_R	4.02	Occipital_Mid_R	96.30
Thalamus_R	3.89	Hippocampus_R	95.24
Occipital_Sup_R	3.85	Supp_Motor_Area_R	87.15
Cuneus_R	3.19	Occipital_Inf_R	83.16
Frontal_Mid_R	3.18	Occipital_Sup_R	80.91
Temporal_Pole_Mid_R	3.00	Thalamus_R	74.63
Fusiform_R	2.69	ParaHippocampal_R	72.08
ParaHippocampal_R	2.31	Frontal_Sup_Orb_R	65.66
Parietal_Sup_R	2.12	Cuneus_R	64.38
Frontal_Mid_Orb_R	1.89	Cingulum_Mid_R	63.26
Olfactory_R	1.53	Parietal_Sup_R	58.84
Frontal_Sup_R	1.31	Fusiform_R	54.21
Supp_Motor_Area_R	1.14	Cingulum_Ant_R	53.35
Precuneus_R	1.06	Calcarine_R	53.28
Cingulum_Mid_R	1.06	Lingual_R	47.74
Frontal_Sup_Orb_R	1.02	Paracentral_Lobule_R	47.61
Cingulum_Ant_R	0.97	Olfactory_R	40.16
Paracentral_Lobule_R	0.84	Precuneus_R	31.55
Frontal_Med_Orb_R	0.74	Frontal_Med_Orb_R	24.94
Frontal_Sup_Medial_R	0.66	Frontal_Sup_Medial_R	22.46
Rectus_R	0.65	Rectus_R	21.97
Cingulum_Post_R	0.30	Cingulum_Post_R	5.07
White matter fibers			
Inf occ-frontal fascicle	21.33	Corticospinal tract	129.20
Uncinate fascicle	20.55	Acoustic radiation	120.77
Acoustic radiation	19.40	Sup longitudinal fascicle	119.70
Sup occ-frontal fascicle	19.16	Inf occ-frontal fascicle	114.87
Sup longitudinal fascicle	15.99	Callosal body	114.47
Corticospinal tract	9.86	Uncinate fascicle	110.66
Optic radiation	8.56	Sup occ-frontal fascicle	109.94
Callosal body	4.78	Optic radiation	81.06

4. Discussion

Based on a representative patient sample of 439 acute right hemisphere stroke patients, we found highest frequencies of overlap for ischemic infarcts in the insula, putamen, operculum and superior temporal cortex. The maximum overlay of hemorrhages was located more posteriorly and more medially, involving posterior areas of the insula, Heschl's gyrus, and putamen.

Our results differ from those by Caviness et al. who investigated a sample of 21 patients with MCA infarction (Caviness et al., 2002). Beyond a center of affection around the sylvian fissure that included pre- and post-central gyri, they observed maxima of lesion frequency in frontal and temporo-occipital areas. The difference could be due to sample size as well as patient selection criteria; Caviness et al. only included stroke patients with dysphasic disturbances. More similarity exists between our results and those reported by Phan et al. (2005). Their aim was to evaluate the boundaries of the MCA territory and thus restricted the included patients to only those with large artery thrombotic

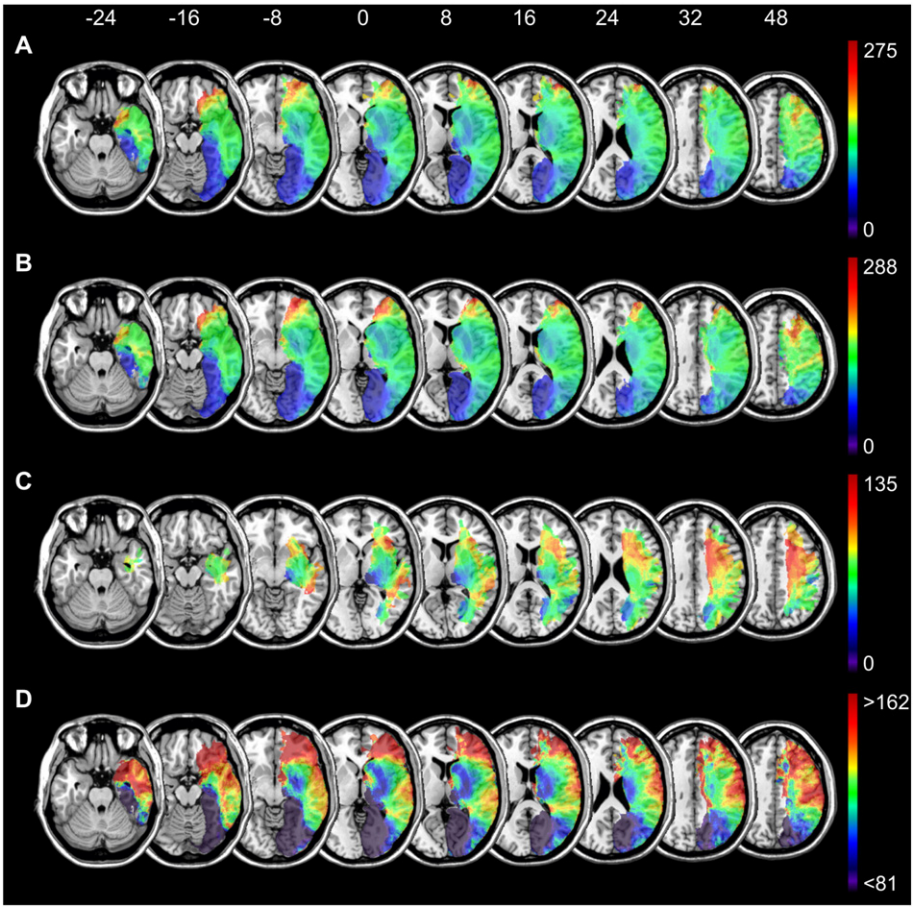

Fig. 2. Lesion size topographies in cm^2 for each voxel lesioned in at least five patients for (A) all 439 acute right brain damaged patients, (B) for infarcts only ($n = 367$), and (C) for hemorrhages only ($n = 72$), each scaled to show the complete possible range from zero to maximal average lesion size. Panel (D) shows average lesion size for all 439 acute right brain damaged patients (same data as in panel A), but with the color-coding rescaled to more effectively visualize variation that is not visible with the color-coding in panel A, especially the variability of lesion size within the territory of the MCA.

MCA stroke. Comparable with our findings they observed highest levels of affection in the striatocapsular area, the insula, and adjacent white matter.

As the documentation of lesion topography in the study of Mah et al. (2014) was limited to a visual illustration of the overlay map, comparisons with the present data can only be made by approximation. In general, lesion topography appears similar to our dataset. One difference appears to be that highest frequency peaks were located around z-slice 20 in MNI-space, while our data set revealed highest frequency peaks more inferiorly. For example, we obtained the absolute maximum of lesion frequency in infarcts ($n = 119$) on z-slices 6, 8, and 9. This might be due to differences in patient selection criteria. While Mah et al. included only patients who had obtained diffusion weighted MR imaging, our study included all stroke patients admitted to our center, and independent of the imaging modality (CT or MR) applied at admission. Linked to this issue there might also be differences in the type of strokes included in the two studies. In many stroke centers, patients with severe and clear stroke symptoms at admission (and thus potentially larger brain areas affected) are examined by CT rather than MR imaging (see introduction chapter above). Thus, it is possible that in a study relying selectively on MR diffusion imaging as the one by Mah et al., lesions of larger volume might be underrepresented and – vice versa – smaller, punctual stroke overrepresented. In fact, lacunar strokes are often found especially in the putamen and in cerebral white matter, (Alistair Lammie, 2000; Benavente et al., 2014) i.e. in those areas where the study by Mah et al. (2014) observed lesion frequency maxima.

Although we consider the inclusion of both CT and MR imaging as essential for our study, this procedure also comes with possible drawbacks. The demarcation of stroke is a dynamic process and imaging modalities differ in their capability to demonstrate damaged tissue at different time points after stroke onset (Welch et al., 2000). Therefore, lesion size estimates might be biased between imaging modalities. Moreover CT imaging, compared to MR imaging, provides a lower resolution and is more prone to artifacts (Audebert and Fiebach, 2015), while diffusion weighted MR imaging in the hyper-acute phase might slightly overstate final lesion size, etc. However, these methodological constrains inherent in our data sample should have non-systematic effects with respect to anatomy, i.e. should occur without a systematic bias in anatomical localization that would favor particular anatomical structures over others.

To conclude, by using a large, representative stroke patient sample the present study accumulated the different sub-patterns of stroke lesions related to the vascularisation of the brain to identify a global stroke pattern in right brain damaged individuals. The middle cerebral artery is the artery which is known to be the most susceptible to occlusion. (e.g., Caplan et al., 1986) Not surprisingly, the present study observed the highest frequencies of affection within the media territory. However, as the present study has also shown, there are different loci inside the vascular territory of the middle cerebral artery that differ in their susceptibility to stroke. The present study offers detailed anatomical information on this pattern, allowing clinicians and researchers to refer to a representative topography of acute stroke.

Disclosures

The authors have no conflicts of interest to report.

Acknowledgments

This work was supported by the Deutsche Forschungsgemeinschaft (KA1258/10-1, KA1258/20-1) and the Open Access Publishing Fund of the University of Tübingen. The authors thank the staff of the Division of Neuropsychology at Tübingen University who helped to collect and preprocess the imaging data; in particular, Bianca de Haan, Johannes Rennig, Urszula Mihulowicz, Julia Suchan, and Dongyun Li.

Appendix A. Supplementary data

Supplementary data to this article can be found online at http://dx.doi.org/10.1016/j.nicl.2015.11.012.

References

Alistair Lammie, G., 2000. Pathology of small vessel stroke. Br. Med. Bull. 56 (2), 296–306.
Audebert, H.J., Fiebach, J.B., 2015. Brain imaging in acute ischemic stroke-MRI or CT? Curr. Neurol. Neurosci. Rep. 15 (3), 526.
Bates, E., Wilson, S.M., Saygin, A.P., Dick, F., Sereno, M.I., et al., 2003. Voxel-based lesion-symptom mapping. Nat. Neurosci. 6, 448–450.
Benavente, O.R., Pearce, L., Bazan, C., Roldan, A.M., Catanese, L., Bhat Livezey, V.M., et al., 2014. Clinical-MRI correlations in a multiethnic cohort with recent lacunar stroke: the SPS3 trial. Int. J. Stroke 9 (8), 1057–1064.
Bürgel, U., Amunts, K., Hoemke, L., Mohlberg, H., Gilsbach, J.M., Zilles, K., 2006. White matter fiber tracts of the human brain: three-dimensional mapping at microscopic resolution, topography and intersubject variability. NeuroImage 29, 1092–1105.
Caplan, L.R., Gorelick, P.B., Hier, D.B., 1986. Race, sex and occlusive cerebrovascular disease: a review. Stroke 17 (4), 648–655.
Caviness, V.S., Makris, N., Montinaro, E., Sahin, N.T., Bates, J.F., et al., 2002. Anatomy of stroke, part i: an MRI-based topographic and volumetric system of analysis. Stroke 33, 2549–2556.
Lee, E., Kang, D.-W., Kwon, S.U., Kim, J.S., 2009. Posterior cerebral artery infarction: diffusion-weighted MRI analysis of 205 patients. Cerebrovasc. Dis. 28, 298–305.
Mah, Y.-H., Husain, M., Rees, G., Nachev, P., 2014. Human brain lesion-deficit inference remapped. Brain 137, 2522–2531.
Mirman, D., Chen, Q., Zhang, Y., Wang, Z., Faseyitan, O.K., Coslett, et al., 2015. Neural organization of spoken language revealed by lesion-symptom mapping. Nat. Commun. 6, 6762.
Neumann-Haefelin, T., Wenserski, F., Siebler, M., 1999. The DWI/PWI mismatch region in acute stroke. Stroke 30, 1591–1597.
Phan, T.G., Donnan, G. a, Wright, P.M., Reutens, D.C., 2005. A digital map of middle cerebral artery infarcts associated with middle cerebral artery trunk and branch occlusion. Stroke 36, 986–991.
Phan, T.G., Fong, A.C., Donnan, G., Reutens, D.C., 2007. Digital map of posterior cerebral artery infarcts associated with posterior cerebral artery trunk and branch occlusion. Stroke 38, 805–811.
Rorden, C., Karnath, H.-O., Bonilha, L., 2007. Improving lesion-symptom mapping. J. Cogn. Neurosci. 19, 1081–1088.
Rorden, C., Bonilha, L., Fridriksson, J., Bender, B., Karnath, H.-O., 2012. Age-specific CT and MRI templates for spatial normalization. NeuroImage 61, 957–965.
Stoeckel, M.C., Wittsack, H.-J., Meisel, S., Seitz, R.J., 2007. Pattern of cortex and white matter involvement in severe middle cerebral artery ischemia. J. Neuroimaging 17, 131–140.
Tzourio-Mazoyer, N., Landeau, B., Papathanassiou, D., Crivello, F., Etard, O., Delacroix, N., et al., 2002. Automated anatomical labeling of activations in SPM using a macroscopic anatomical parcellation of the MNI MRI single-subject brain. NeuroImage 15, 273–289.
Welch, K.M.A., Cao, Y., Nagesh, V., 2000. Magnetic resonance assessment of acute and chronic stroke. Prog. Cardiovasc. Dis. 43 (2), 113–134.